

Energy-efficient 8-point DCT Approximations: Theory and Hardware Architectures

Renato J. Cintra* Fábio M. Bayer† Vitor A. Coutinho ‡ Sunera Kulasekera
Arjuna Madanayake§

Abstract

Due to its remarkable energy compaction properties, the discrete cosine transform (DCT) is employed in a multitude of compression standards, such as JPEG and H.265/HEVC. Several low-complexity integer approximations for the DCT have been proposed for both 1-D and 2-D signal analysis. The increasing demand for low-complexity, energy efficient methods require algorithms with even lower computational costs. In this paper, new 8-point DCT approximations with very low arithmetic complexity are presented. The new transforms are proposed based on pruning state-of-the-art DCT approximations. The proposed algorithms were assessed in terms of arithmetic complexity, energy retention capability, and image compression performance. In addition, a metric combining performance and computational complexity measures was proposed. Results showed good performance and extremely low computational complexity. Introduced algorithms were mapped into systolic-array digital architectures and physically realized as digital prototype circuits using FPGA technology and mapped to 45 nm CMOS technology. All hardware-related metrics showed low resource consumption of the proposed pruned approximate transforms. The best proposed transform according to the introduced metric presents a reduction in power consumption of 21–25%.

Keywords

DCT approximation image compressionFPGA pruned transforms

1 INTRODUCTION

Transform-based methods are widely employed in digital signal processing applications [1]. In this context, the efficient computation of discrete transforms has constantly attracted community efforts and the proposition of fast algorithms [2]. In particular, the 8-point discrete cosine transform (DCT) has a proven record of scientific and industrial applications, as demonstrated by the multitude of image and video coding standards that adopt it, such as: JPEG [3], MPEG [4–6], H.261 [7, 8], H.263 [5, 9], H.264/AVC [10, 11], and the recent high efficiency video coding (HEVC) [12, 13]. The HEVC is capable of achieving high compression

*Renato J. Cintra is with the Signal Processing Group, Departamento de Estatística, Universidade Federal de Pernambuco, Recife, PE, Brazil; Equipe Cairn, IRISA-INRIA, Université de Rennes 1, Rennes, France; LIRIS, Institut National des Sciences Appliquées, Lyon, France (e-mail: rjdesc@stat.ufpe.org).

†Fábio M. Bayer is with the Departamento de Estatística and LACESM, Universidade Federal de Santa Maria, Santa Maria, RS, Brazil (e-mail: bayer@ufsm.br).

‡Vitor A. Coutinho is with the Graduate Program in Electrical Engineering and the Signal Processing Group, Departamento de Estatística, Universidade Federal de Pernambuco, Recife, PE, Brazil (e-mail: vitor.andrade.coutinho@gmail.com).

§Sunera Kulasekera and Arjuna Madanayake are with the Department of Electrical and Computer Engineering, The University of Akron, Akron, OH, USA (e-mail: arjuna@uakron.edu).

performance at approximately half the bit rate required by its predecessor H.264/AVC with same image quality [13–16]. On the other hand, the HEVC requires a significantly higher computational complexity in terms of arithmetic operations [14–17], being 2–4 times more computationally costly than H.264/AVC [14, 16]. In this context, the efficient computation of the DCT is a venue for improving the performance of above-mentioned codecs.

Since its inception, several fast algorithms for the DCT have been proposed [18–23]. However, traditional algorithms aim at the computation of the *exact* DCT, which requires several multiplication operations. Additionally, several algorithms have achieved theoretical multiplicative complexity lower-bounds [21, 24]. As a consequence, the progress in this area headed to approximate methods [25–27]. In some applications, a simple DCT approximation can provide meaningful results at low arithmetic complexity [28]. Thus, approximation techniques for the DCT are becoming increasingly popular [25, 27, 29–31]. Such approximations can reduce the computational demands of the DCT, leading to low-power, high-speed realizations [16], while ensuring adequate numerical accuracy.

Furthermore, it is a well-known fact that in many DCT applications [32–34], the most useful signal information tends to be concentrated in the low-frequency coefficients. This is because the DCT presents good energy compaction properties, which are closely related to the Karhunen-Loève transform [35]. Therefore, only the low-frequency DCT components are necessary to be computed in these applications. A typical example of this situation occurs in data compression applications [36], where high-frequency components are often zeroed by the quantization process [37, p. 586]. Then, only the quantities that are likely to be significant should be computed [38]. This approach is called frequency-domain *pruning* and has been employed for computing the discrete Fourier transform (DFT) [39–43]. Such methodology was originally applied in the DCT context in [44] and [45]. In [32, 46], the two-dimensional (2-D) version of the pruned DCT was proposed. In the context of low-powered wireless vision sensor networks, a pruned DCT was proposed in [47] based on the binary DCT [30].

In [48], Meher *et al.* proposed a HECV architecture where the wordlength was maintained fixed by means of discarding least significant bits. In that context, the goal was the minimization of the computation complexity at the expense of wordlength truncation. Such approach was also termed ‘pruning’. However, it is fundamentally different from the approach discussed in the current paper. This terminology distinction is worth observing.

Thus, in response to the growing need for high compression of image and moving pictures for various applications [12], we propose a further reduction of the computational cost of the 8-point DCT computation in the context of JPEG-like compression and HEVC processing. In this work, we introduce pruned DCT approximations for image and video compression. Essentially, DCT-like pruning consists of extracting from a given approximate DCT matrix a submatrix that aims at furnishing similar mathematical properties. We advance the application of pruning techniques to several DCT approximations listed in recent literature. In this paper, we aim at identifying adequate pruned approximations for image compression applications. VLSI realizations of both 1-D and 2-D of the proposed methods are also sought.

This paper is organized as follows. In Section 2, a mathematical review of DCT approximation and pruning methods is furnished. Exact and approximate DCT are presented and the pruning procedure is mathematically described. In Section 3, we propose several pruned methods for approximate DCT computation and assess them by means of arithmetic complexity, coefficient energy distribution in transform-domain,

and image compression performance. A combined figure of merit considering performance and complexity is introduced. In Section 4, a VLSI realization of the optimum pruned method according to the suggested figure of merit is proposed. Both FPGA and ASIC realizations are assessed in terms of area, time, frequency, and power consumption. Section 5 concludes the paper.

2 MATHEMATICAL BACKGROUND

2.1 DISCRETE COSINE TRANSFORM

Let $\mathbf{x} = [x_0 \ x_1 \ \cdots \ x_{N-1}]^\top$ be an N -point input vector. The one-dimensional DCT is a linear transformation that maps \mathbf{x} into an output vector $\mathbf{X} = [X_0 \ X_1 \ \cdots \ X_{N-1}]^\top$ of transform coefficients, according to the following expression [49]:

$$X_k = \alpha_k \cdot \sqrt{\frac{2}{N}} \cdot \sum_{n=0}^{N-1} x_n \cdot \cos \left\{ \frac{(n + \frac{1}{2})k\pi}{N} \right\}, \quad (1)$$

where $k = 0, 1, \dots, N-1$, $\alpha_0 = 1/\sqrt{2}$ and $\alpha_k = 1$, for $k > 0$. In matrix formalism, (1) is given by:

$$\mathbf{X} = \mathbf{C} \cdot \mathbf{x}, \quad (2)$$

where \mathbf{C} is the N -point DCT matrix whose entries are expressed according $c_{m,n} = \alpha_m \cdot \sqrt{2/N} \cdot \cos \{(n + \frac{1}{2})m\pi/N\}$, $m, n = 0, 1, \dots, N-1$ [23]. Being an orthogonal transform, the inverse transformation is given by: $\mathbf{x} = \mathbf{C}^\top \cdot \mathbf{X}$. Because DCT satisfies the kernel separability property, the 2-D DCT can be expressed in terms of the 1-D DCT. Let \mathbf{A} be an $N \times N$ matrix. The forward 2-D DCT operation applied to \mathbf{A} yields a transform-domain image \mathbf{B} furnished by: $\mathbf{B} = \mathbf{C} \cdot \mathbf{A} \cdot \mathbf{C}^\top$. In fact, the 2-D DCT can be computed after eight column-wise calls of the 1-D DCT to \mathbf{A} ; then the resulting intermediate image is submitted to eight row-wise calls of the 1-D DCT. In this paper, we devote our attention to the case $N = 8$.

2.2 DCT APPROXIMATIONS

In general terms, a DCT approximation $\hat{\mathbf{C}}$ is constituted of the product a low-complexity matrix \mathbf{T} and a scaling diagonal matrix \mathbf{S} that ensures orthogonality or quasi-orthogonality [31]. Thus, we have $\hat{\mathbf{C}} = \mathbf{S} \cdot \mathbf{T}$ [16, 27, 28, 50]. The entries of the low-complexity matrix are defined over the set $\{0 \pm 1, \pm 2\}$, which results in a multiplierless operator—only addition and bit-shifting operations are required. Usually possessing irrational elements, the scaling diagonal matrix \mathbf{S} does not pose any extra computation overhead for image and video compression applications. This is due to the fact that the matrix \mathbf{S} can be conveniently merged into the quantization step of compression algorithms [16, 27, 29, 50].

Among the various DCT approximations archived in literature, we separate the following methods: (i) the signed DCT (SDCT), which is the seminal method in the DCT approximation field [25]; (ii) Bouguezel-Ahmad-Swamy approximations [27, 29, 30]; (iii) the rounded DCT (RDCT) [28], and (iv) the modified RDCT (MRDCT) [50]. These approximations were selected because they collectively exhibit a wide range of complexity vs. performance trade-off figures [50]. Moreover, such approximations have been demonstrated to be useful in image compression. The low-complexity matrices of above methods are shown in Table 1. Ad-

Table 1: Approximate DCT methods

Method	T	Orthogonal?
SDCT [25]	$\begin{bmatrix} 1 & 1 & 1 & 1 & 1 & 1 & 1 & 1 \\ 1 & 1 & 1 & 1 & -1 & -1 & -1 & -1 \\ 1 & 1 & -1 & -1 & -1 & -1 & 1 & 1 \\ 1 & -1 & -1 & -1 & 1 & 1 & 1 & -1 \\ 1 & -1 & -1 & 1 & 1 & -1 & -1 & 1 \\ 1 & -1 & 1 & 1 & -1 & -1 & 1 & -1 \\ 1 & -1 & 1 & -1 & -1 & 1 & -1 & 1 \\ 1 & -1 & 1 & -1 & 1 & -1 & 1 & -1 \end{bmatrix}$	No
WHT [51]	$\begin{bmatrix} 1 & 1 & 1 & 1 & 1 & 1 & 1 & 1 \\ 1 & 1 & 1 & 1 & -1 & -1 & -1 & -1 \\ 1 & 1 & -1 & -1 & 1 & 1 & -1 & -1 \\ 1 & -1 & -1 & 1 & 1 & -1 & -1 & 1 \\ 1 & 1 & 1 & 1 & -1 & -1 & -1 & -1 \\ 1 & -1 & 1 & -1 & -1 & 1 & -1 & 1 \\ 1 & 1 & -1 & -1 & -1 & -1 & 1 & 1 \\ 1 & -1 & -1 & 1 & -1 & 1 & 1 & -1 \end{bmatrix}$	Yes
BAS-2008 [27]	$\begin{bmatrix} 1 & 1 & 1 & 1 & 1 & 1 & 1 & 1 \\ 1 & 1 & 0 & 0 & 0 & 0 & -1 & -1 \\ 1 & \frac{1}{2} & -\frac{1}{2} & -1 & -1 & -\frac{1}{2} & \frac{1}{2} & 1 \\ 0 & 0 & -1 & 0 & 0 & 1 & 0 & 0 \\ 1 & -1 & -1 & 1 & 1 & -1 & -1 & 1 \\ 1 & -1 & 0 & 0 & 0 & 0 & 1 & -1 \\ \frac{1}{2} & -1 & 1 & -\frac{1}{2} & -\frac{1}{2} & 1 & -1 & \frac{1}{2} \\ 0 & 0 & 0 & -1 & 1 & 0 & 0 & 0 \end{bmatrix}$	Yes
BAS-2009 [29]	$\begin{bmatrix} 1 & 1 & 1 & 1 & 1 & 1 & 1 & 1 \\ 1 & 1 & 0 & 0 & 0 & 0 & -1 & -1 \\ 1 & 1 & -1 & -1 & -1 & -1 & 1 & 1 \\ 0 & 0 & -1 & 0 & 0 & 1 & 0 & 0 \\ 1 & -1 & -1 & 1 & 1 & -1 & -1 & 1 \\ 1 & -1 & 0 & 0 & 0 & 0 & 1 & -1 \\ 1 & -1 & 1 & -1 & -1 & 1 & -1 & 1 \\ 0 & 0 & 0 & -1 & 1 & 0 & 0 & 0 \end{bmatrix}$	Yes
BAS-2013 [30]	$\begin{bmatrix} 1 & 1 & 1 & 1 & 1 & 1 & 1 & 1 \\ 1 & 1 & 1 & 1 & -1 & -1 & -1 & -1 \\ 1 & 1 & -1 & -1 & -1 & -1 & 1 & 1 \\ 1 & 1 & -1 & -1 & 1 & 1 & -1 & -1 \\ 1 & -1 & -1 & 1 & 1 & -1 & -1 & 1 \\ 1 & -1 & -1 & 1 & -1 & 1 & 1 & -1 \\ 1 & -1 & 1 & -1 & -1 & 1 & -1 & 1 \\ 1 & -1 & 1 & -1 & 1 & -1 & 1 & -1 \end{bmatrix}$	Yes
RDCT [28]	$\begin{bmatrix} 1 & 1 & 1 & 0 & 0 & -1 & -1 & -1 \\ 1 & 0 & 0 & -1 & -1 & 0 & 0 & 1 \\ 1 & 0 & -1 & -1 & 1 & 1 & 0 & -1 \\ 1 & -1 & -1 & 1 & 1 & -1 & -1 & 1 \\ 1 & -1 & 0 & 1 & -1 & 0 & 1 & -1 \\ 0 & -1 & 1 & 0 & 0 & 1 & -1 & 0 \\ 0 & -1 & 1 & -1 & 1 & -1 & 1 & 0 \\ 1 & 1 & 1 & 1 & 1 & 1 & 1 & 1 \end{bmatrix}$	Yes
MRDCT [50]	$\begin{bmatrix} 1 & 1 & 1 & 1 & 1 & 1 & 1 & 1 \\ 1 & 0 & 0 & 0 & 0 & 0 & 0 & -1 \\ 1 & 0 & 0 & -1 & -1 & 0 & 0 & 1 \\ 0 & 0 & -1 & 0 & 0 & 1 & 0 & 0 \\ 1 & -1 & -1 & 1 & 1 & -1 & -1 & 1 \\ 0 & -1 & 0 & 0 & 0 & 0 & 1 & 0 \\ 0 & -1 & 1 & 0 & 0 & 1 & -1 & 0 \\ 0 & 0 & 0 & -1 & 1 & 0 & 0 & 0 \end{bmatrix}$	Yes

ditionally, we also considered the 8-point naturally ordered Walsh-Hadamard transform (WHT), which is a well-known low-complexity transform with applications in image processing [30, 51].

2.3 PRUNED EXACT AND APPROXIMATE DCT

Essentially, DCT pruning consists of extracting from the 8×8 DCT matrix \mathbf{C} a submatrix that aims at furnishing similar mathematical properties as \mathbf{C} . Pruning is often realized on the transform-domain by means of computing fewer transform coefficients than prescribed by the full transformation. Usually, only the $K < N$ coefficients that retain more energy are preserved. For the DCT, this corresponds to the first K

rows of the DCT matrix. Therefore, this particular type of pruning implies the following $K \times 8$ matrix:

$$\mathbf{C}_K = \begin{bmatrix} c_{0,0} & c_{0,1} & \cdots & c_{0,7} \\ c_{1,0} & c_{1,1} & \cdots & c_{1,7} \\ \vdots & \vdots & \ddots & \vdots \\ c_{K-1,0} & c_{K-1,1} & \cdots & c_{K-1,7} \end{bmatrix}, \quad (3)$$

where $0 < K \leq 8$ and $c_{m,n}$, $m, n = 0, 1, \dots, 7$, are the entries of \mathbf{C} . The case $K = 8$ corresponds to the original transformation. Such procedure was proposed in [32,46] for the DCT in the context of wireless sensor networks. For the 2-D case, we have that the pruned DCT is given by: $\tilde{\mathbf{B}} = \mathbf{C}_K \cdot \mathbf{A} \cdot \mathbf{C}_K^\top$. Notice that $\tilde{\mathbf{B}}$ is a $K \times K$ matrix over the transform-domain. Lecuire *et al.* [46] showed that retaining the transform-domain coefficients in a $K \times K$ square pattern at the upper-right corner leads to a better energy-distortion trade-off when compared to the alternative triangle pattern [32].

The pruning approach can be applied to DCT approximations. By discarding the lower rows of the low-complexity matrix \mathbf{T} , we obtain the following $K \times N$ pruned matrix transformation:

$$\mathbf{T}_K = \begin{bmatrix} t_{0,0} & t_{0,1} & \cdots & t_{0,7} \\ t_{1,0} & t_{1,1} & \cdots & t_{1,7} \\ \vdots & \vdots & \ddots & \vdots \\ t_{K-1,0} & t_{K-1,1} & \cdots & t_{K-1,7} \end{bmatrix}, \quad (4)$$

where $t_{m,n}$, $m, n = 0, 1, \dots, 7$, are the entries of \mathbf{T} (cf. Table 1). Considering the orthogonalization method described in [31], the $K \times 8$ pruned approximate DCT is given by:

$$\hat{\mathbf{C}}_K = \mathbf{S}_K \cdot \mathbf{T}_K, \quad (5)$$

where $\mathbf{S}_K = \sqrt{\text{diag}\{(\mathbf{T}_K \cdot \mathbf{T}_K^\top)^{-1}\}}$ is a $K \times K$ diagonal matrix and $\text{diag}(\cdot)$ returns a diagonal matrix with the diagonal elements of its argument. If \mathbf{T} is orthogonal, then \mathbf{T}_K satisfies semi-orthogonality [52, p. 84].

The 2-D pruned DCT of a matrix \mathbf{A} is given by

$$\tilde{\mathbf{B}} = \mathbf{T}_K \cdot \mathbf{A} \cdot \mathbf{T}_K^\top. \quad (6)$$

Resulting transform-domain matrix $\tilde{\mathbf{B}}$ is sized $K \times K$.

3 COMPLEXITY AND PERFORMANCE ASSESSMENT

In this section, we analyze the arithmetic complexity of the selected pruned DCT approximations. We also assess their performance in terms of energy retention and image compression for each value of K .

3.1 ARITHMETIC COMPLEXITY

Because all considered approximate DCT are natively multiplierless operators, the pruned DCT approximation inherits such property. Therefore, the arithmetic complexity of the pruned approximations is simply

given by the number of additions and bit-shifting operations required by their respective fast algorithms. To illustrate the complexity assessment, we focus on the MRDCT [50], whose fast algorithm signal flow graph (SFG) is shown in Figure 1(a). The full computation of the MRDCT requires 14 additions. By judiciously considering the computational cost of only the first K transform-domain components, we derived fast algorithms for the pruned MRDCT matrices as shown in Figure 1.

The same procedure was applied to each of the discussed approximations based on their fast algorithms [25, 27–30, 50, 51]. The obtained arithmetic additive complexity is presented in Table 2. We notice that the pruned MRDCT exhibited the lowest computational complexity for all values of K . Such mathematical properties of the MRDCT are translated into good hardware designs. Indeed, in [16], several DCT approximations were physically realized in FPGA devices. Hardware and performance assessments revealed that the MRDCT outperformed several competitors, including BAS 2008 [27] and RDCT [28], in terms of speed, hardware resource consumption, and power consumption [16].

An examination of (6) reveals that the 2-D pruned approximate DCT is computed after eight column-wise calls of the 1-D pruned approximate DCT and K row-wise call of 1-D pruned approximate DCT. Let $A_{1-D}(\mathbf{T}_K)$ be the additive complexity of \mathbf{T}_K . Therefore, the additive complexity of the 2-D pruned approximate DCT is given by:

$$\begin{aligned} A_{2-D}(\mathbf{T}_K) &= 8 \cdot A_{1-D}(\mathbf{T}_K) + K \cdot A_{1-D}(\mathbf{T}_K) \\ &= (8 + K) \cdot A_{1-D}(\mathbf{T}_K). \end{aligned} \tag{7}$$

For the particular case of the pruned MRDCT, we can derive the expressions below:

$$A_{1-D}(\mathbf{T}_K) = K + 6, \tag{8}$$

$$A_{2-D}(\mathbf{T}_K) = K^2 + 14 \cdot K + 48, \tag{9}$$

for $K = 1, 2, \dots, 8$.

3.2 RETAINED ENERGY

To further examine the performance of the pruned approximations, we investigate the signal energy distribution in the transform-domain for each value of K . This analysis is relevant, because higher energy concentrations implies that K can be reduced without severely degrading the transform coding performance [23]. In fact, higher energy concentration effects a large number of zeros in the transform-domain after quantization. On its turn, a large number of zeros translates into longer runs of zeros, which are beneficial for subsequent run-length encoding and Huffman coding stages [53].

We analyzed a set of fifty 512×512 256-level grayscale standard images from [54]. Originally color images were converted to grayscale by extracting the luminance. Image types included textures, satellite images, landscapes, portraits, and natural images. Such variety is to ensure that selection bias is not introduced in our experiments. Thus our results are expected to be robust in this sense. Images were split into 8×8 subimages. Resulting subimages were submitted to each of the discussed pruned DCT approximation for all values of K . Subsequently, the relative amount of retained energy in the transform-domain was computed. Obtained values are displayed in Table 2.

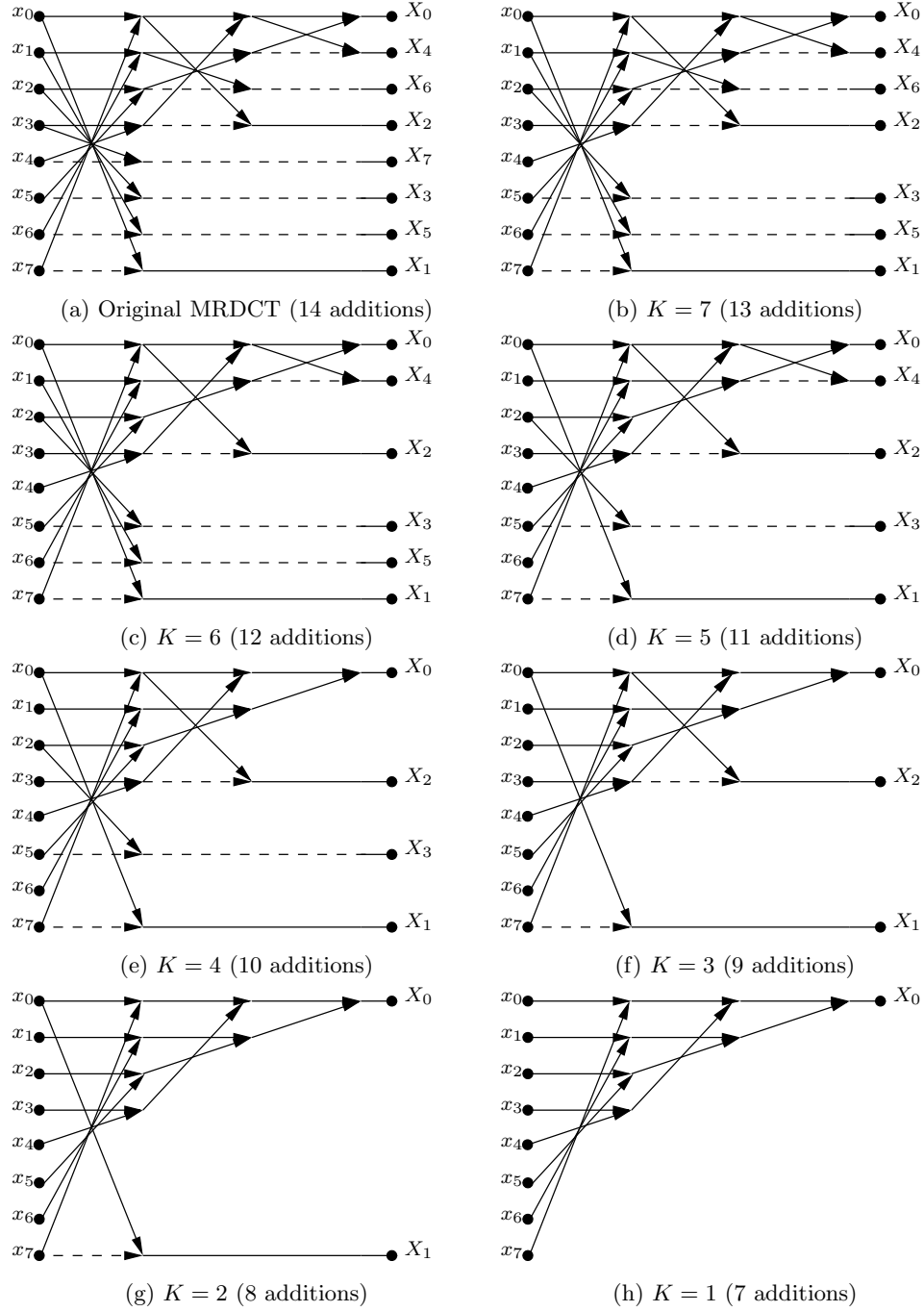


Figure 1: Signal flow graph for the MRDCT matrix and pruned MRDCT matrices

Table 2: Complexity and performance assessment of pruned DCT approximations

Measure	Method	K							
		1	2	3	4	5	6	7	8
Additive complexity	Exact DCT [32]	7	20	23	24	25	26	28	29
	WHT [51]	7	8	11	12	19	20	23	24
	SDCT [25]	7	14	17	19	20	22	23	24
	BAS-2008 [27]	7	10	13	14	15	16	17	18
	BAS-2009 [29]	7	10	13	14	15	16	17	18
	BAS-2013 [30, 47]	7	14	17	20	21	22	23	24
	RDCT [28]	7	12	13	16	17	19	20	22
	MRDCT [50]	7	8	9	10	11	12	13	14
Mean retained energy	Exact DCT	95.46	97.47	98.55	99.13	99.49	99.71	99.87	100.00
	WHT	95.46	95.57	96.03	96.25	98.24	98.52	99.63	100.00
	SDCT	95.46	96.39	97.30	98.16	98.52	99.26	99.61	100.00
	BAS-2008	95.46	97.08	98.10	98.86	99.20	99.51	99.68	100.00
	BAS-2009	95.46	97.08	97.96	98.71	99.04	99.35	99.68	100.00
	BAS-2013	95.46	97.18	98.08	98.76	99.10	99.44	99.77	100.00
	RDCT	95.46	97.36	98.28	98.81	99.16	99.41	99.75	100.00
	MRDCT	95.46	96.41	97.22	97.91	98.22	99.34	99.68	100.00
Mean PSNR	Exact DCT	23.17	26.08	28.52	30.40	31.71	32.39	32.78	33.12
	WHT	23.17	23.17	23.63	23.81	26.88	27.22	29.40	30.17
	SDCT	23.17	24.28	25.23	27.15	27.59	28.43	28.82	29.84
	BAS-2008	23.17	25.30	27.04	29.34	30.15	30.97	31.33	32.20
	BAS-2009	23.17	25.30	26.95	28.70	29.47	30.14	30.96	31.76
	BAS-2013	23.17	24.41	26.95	28.73	29.51	30.31	31.12	31.84
	RDCT	23.17	25.83	27.64	28.94	29.79	30.41	31.21	31.96
	MRDCT	23.17	24.29	25.26	26.37	26.77	29.58	30.29	30.98
Mean SSIM	Exact DCT	0.48	0.66	0.79	0.86	0.89	0.90	0.90	0.90
	WHT	0.48	0.49	0.55	0.58	0.74	0.76	0.82	0.83
	SDCT	0.48	0.59	0.67	0.77	0.80	0.81	0.82	0.84
	BAS-2008	0.48	0.62	0.74	0.83	0.85	0.87	0.88	0.89
	BAS-2009	0.48	0.62	0.73	0.82	0.84	0.85	0.87	0.88
	BAS-2013	0.48	0.64	0.74	0.82	0.85	0.87	0.87	0.88
	RDCT	0.48	0.66	0.76	0.82	0.85	0.87	0.88	0.88
	MRDCT	0.48	0.55	0.65	0.72	0.76	0.83	0.84	0.86
Mean SR-SIM	Exact DCT	0.816	0.953	0.988	0.995	0.995	0.996	0.997	0.997
	WHT	0.815	0.815	0.823	0.823	0.955	0.955	0.982	0.982
	SDCT	0.816	0.943	0.971	0.986	0.986	0.994	0.994	0.994
	BAS-2008	0.816	0.936	0.973	0.993	0.993	0.993	0.993	0.995
	BAS-2009	0.816	0.936	0.974	0.993	0.993	0.993	0.993	0.995
	BAS-2013	0.815	0.951	0.982	0.997	0.997	0.997	0.997	0.997
	RDCT	0.816	0.952	0.981	0.988	0.988	0.988	0.992	0.993
	MRDCT	0.816	0.898	0.932	0.958	0.958	0.982	0.986	0.988

3.3 IMAGE COMPRESSION

Proposed methods were submitted to an image compression simulation to facilitate their performance as an image/video coding tool. We based our experiments on the image compression simulation described in [25, 27, 36, 53, 55], which is briefly outlined next. We considered the same above-mentioned set of images, sub-image decomposition, and 2-D pruned transformation, as detailed in previous sub-section. Resulting data were quantized by dividing each term of the transformed matrix by elements of the standard quantization matrix for luminance [53, p. 153]. Differently from [25, 27, 28], we included the quantization step in image compression simulation. This is a more realistic and suitable approach for pruned methods which take advantage of quantization step.

An inverse procedure was applied to reconstruct images considering 2-D inverse transform operation. Recovered images were assessed for image degradation by means of peak signal-to-noise (PSNR) [53, p. 9], structural similarity index (SSIM) [56], and spectral residual based similarity (SR-SIM) [57]. The SSIM compares an original image \mathbf{I} with the recovered image \mathbf{R} according to the following expression:

$$\text{SSIM}(\mathbf{I}, \mathbf{R}) = \frac{[2\mu_I\mu_R + (L \cdot 10^{-2})] \cdot [2\sigma_{IR} + (3L \cdot 10^{-2})]}{[\mu_I^2 + \mu_R^2 + (L \cdot 10^{-2})] \cdot [\sigma_I^2 + \sigma_R^2 + (3L \cdot 10^{-2})]}, \quad (10)$$

where $\mu_I = \sum_{i=1}^8 \sum_{j=1}^8 \omega_{i,j} \cdot \mathbf{I}_{i,j}$, $\sigma_I = \sum_{i=1}^8 \sum_{j=1}^8 \omega_{i,j} \cdot (\mathbf{I}_{i,j} - \mu_I)^{1/2}$, $\sigma_{IR} = \sum_{i=1}^8 \sum_{j=1}^8 \omega_{i,j} \cdot (\mathbf{I}_{i,j} - \mu_I) \cdot (\mathbf{R}_{i,j} - \mu_R)$, $L = 255$ is the dynamic range of pixels values, and $\omega_{i,j}$ is entry of a Gaussian weighting function $\mathbf{w} = [\omega_{i,j}]$, $i, j = 1, 2, \dots, 8$, with standard deviation of 1.5 and normalized to unit sum. The SR-SIM between the original image \mathbf{I} and the recovered image \mathbf{R} is calculated as described in [57].

Average PSNR, SSIM, and SR-SIM values of all images were computed and are shown in Table 2. For a qualitative analysis, Figure 2 displays the reconstructed Lena image computed via the MRDCT for all values of K . Associated PSNR, SSIM, and SR-SIM values are also shown. Visual inspection suggests $K = 6$ as good compromise between quality and complexity. Indeed, we notice that the PSNR improvement from $K = 5$ to $K = 6$ is 3.92 dB, while the PSNR difference from $K = 6$ and $K = 7$ is just 0.4 dB.

3.4 COMBINED ANALYSIS

In order to compare the discussed approximations, we consider a combined figure of merit that takes into account some of the previously discussed measures. Although popular and worth reporting, mean retained energy and PSNR are closely related measures. Similarly, the SR-SIM is a derivative of SSIM. For a combined figure of merit, we aim at selecting unrelated measures; thus we separated the 2-D additive complexity, PSNR, and SSIM values, whose numerical values are listed in Table 2. Such combined measure is proposed as the following linear cost function:

$$\begin{aligned} \text{cost}(\mathbf{T}_K) = & \alpha_1 \cdot \text{A}_{2\text{-D}}(\mathbf{T}_K) + (1 - \alpha_1) \cdot \\ & \left\{ \alpha_2 \cdot [-\text{NMSSIM}(\mathbf{T}_K)] + (1 - \alpha_2) \cdot [-\text{NMPSNR}(\mathbf{T}_K)] \right\}, \end{aligned} \quad (11)$$

where $\alpha_1, \alpha_2 \in [0, 1]$ are weights; and NMSSIM and NMPSNR represent the normalized mean SSIM, and normalized mean PSNR, respectively, for all considered images submitted to a particular approximation \mathbf{T}_K . The above cost function consists of a multi-objective function, which are commonly found in optimization

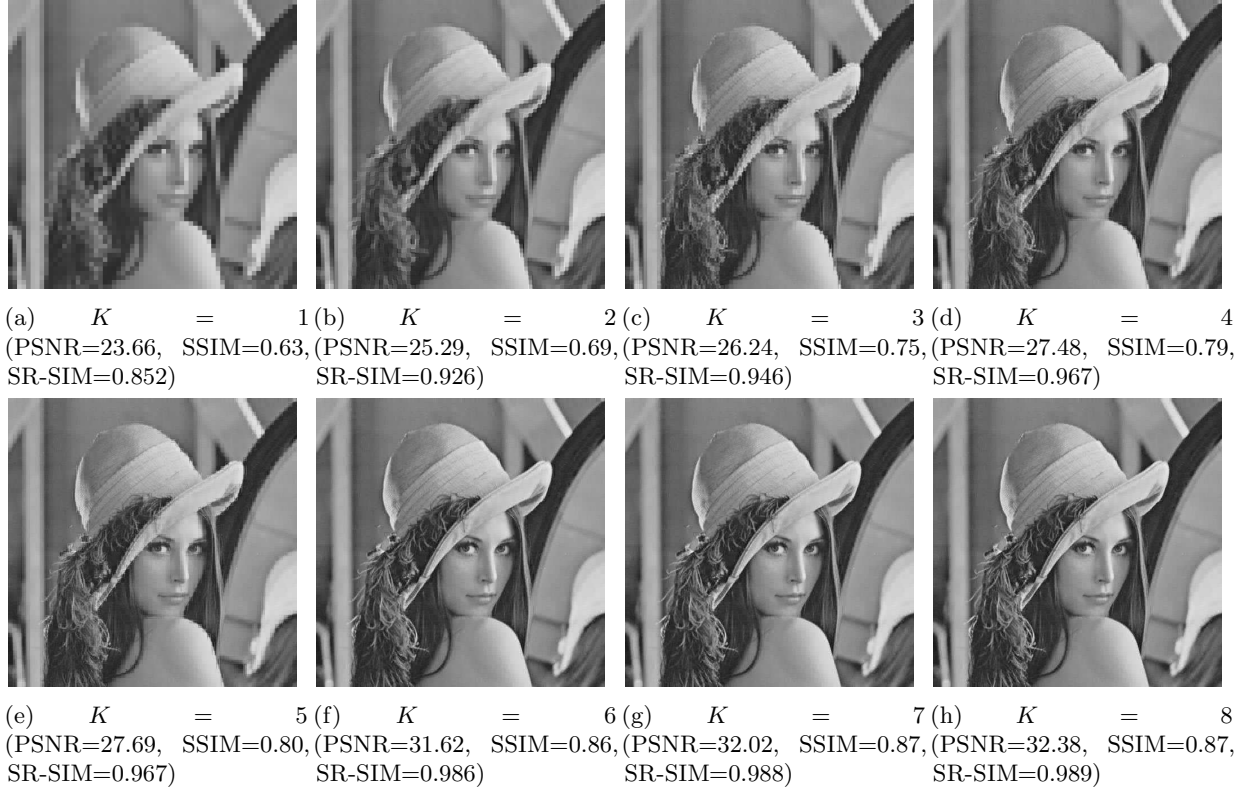


Figure 2: Reconstructed Lena image according to the pruned MRDCT

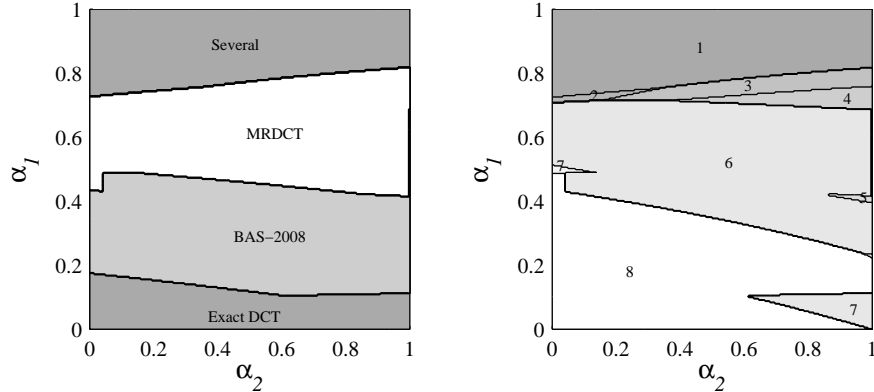


Figure 3: Optimality regions for the cost function: (a) optimal transform and (b) optimal pruning value.

literature [58]. Two types of metrics—arithmetic complexity and performance measurements—are subject to a convex combination according to α_1 . The performance measurements are themselves a convex combination of SSIM and PSNR measurements, balanced according to α_2 . Thus the weights α_1 and α_2 control the relative importance of the constituent metrics of the cost function. For large values of α_1 , the cost function emphasizes the minimization of the computational complexity; whereas, for small values of α_1 , the cost function is prone to capture measures of image quality performance. The quantity α_2 balances the composition of the performance measurement between NMSSIM and NMPSNR. Because we consider $\alpha_1, \alpha_2 \in [0, 1]$, all possible combinations of weights are taken into account. Only the particular context, application, and user requirements can determine the final choice of the weight values.

Figure 3(a) and (b) shows, respectively, regions for optimal transformation and pruning value K , considering any choice of weights values α_1 and α_2 . For large α_1 (emphasis in complex minimization), the optimal choice tends to small K regardless the transform. Indeed, for small K , most pruned transformations collapse to the same matrix. For small α_1 (emphasis in performance maximization), optimality favors more complex transformations with large values of K , being the full exact DCT the limiting case.

For mid-range values of α_1 , we have less trivial scenarios. In Figure 3(a), considering the optimal transform, we notice that for mid-range values of α_1 the MRDCT and the BAS-2008 occupy most of the central area of the discussed region. Around the same region in Figure 3(b), for the MRDCT, we obtain mostly $K = 6$; whereas for the BAS-2008 we have $K = 6, 8$. We emphasize that the proposed pruned MRDCT with $K = 6$ requires *only 12 additions*. The fast algorithm for this particular case is presented in Figure 1(c).

3.5 HEVC SIMULATION

Taking into account the previous combined analysis, we embedded the proposed pruned MRDCT ($K = 6$), the BAS-2008 approximation ($K = 8$), and the pruned BAS-2008 ($K = 6$) in the widely employed HEVC reference software HM 10.0 [59]. This embedding consisted of substituting the original 8-point integer-based DCT transform present in the codec for each of the above-mentioned approximations. We considered nine CIF video sequences with 300 frames at 25 frames per second from a public video bank [60]. Such sequences were submitted to encoding according to: (i) the original software, and (ii) the modified software. We assessed mean PSNR metrics for luminance by varying the quantization parameter (QP) from 10 to 50 with

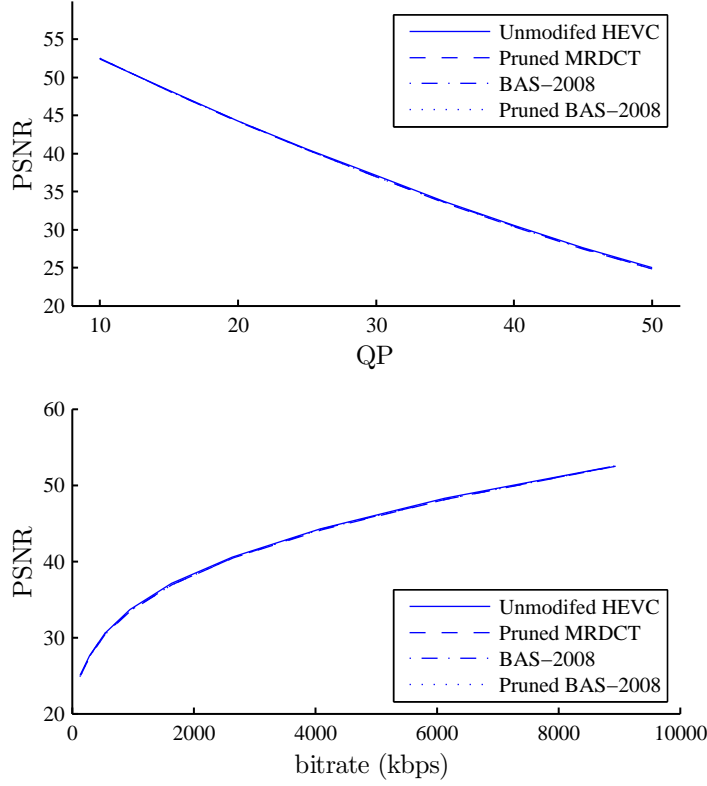
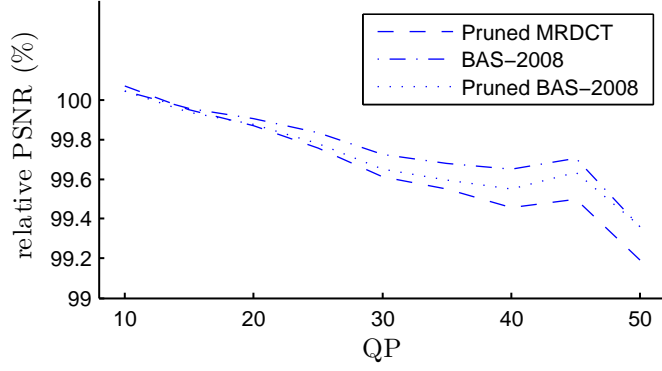


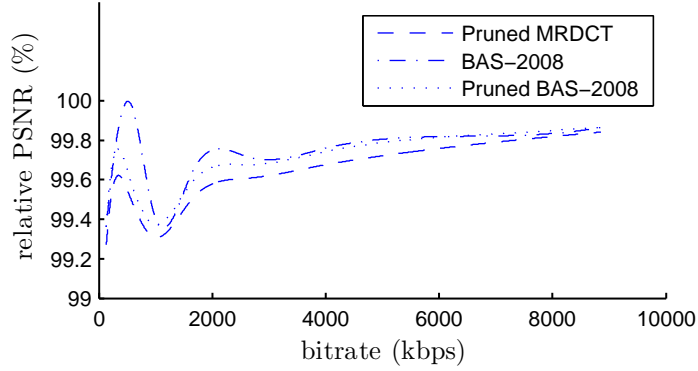
Figure 4: Video coding performance assessment.

steps of 5 units. Results are shown in Figure 4 considering both QP and bitrate. Obtained curves are almost indistinguishable. The mean PSNR values at $QP = 30$ correspond to 37.06 dB, 36.92 dB, 36.96 dB, and 36.93 dB for the original integer DCT, the pruned MRDCT ($K = 6$), BAS-2008, and the pruned BAS-2008 ($K = 6$), respectively. The degradation of the pruned approximations methods relative to the unmodified software was smaller than 0.15 dB for such QP value.

Figure 5 shows the relative percent PSNR of each approximate method compared to the original HEVC according to QP and bitrate values. The curves show very close performance to the original codec. In Figure 5(a), for low QP values, the approximations show even higher PSNR, i.e., more than 100% relative PSNR, suggesting better compaction capability at low compression rates. However, same QP values do not necessarily generate the same compression ratio for each method, since distinct coefficients are derived from each transformation and submitted to the same quantization table. Figure 5(b) indicates that the approximations possess slightly lower coding performance compared to original HEVC when compared at same bitrate. At the same time, the approximate methods present considerable lower computational cost and the lost of performance is smaller than 1%. Figure 6 shows a qualitative comparison considering the first frame of the standard “Foreman” video sequence at $QP = 30$. The degradation is hardly perceived.



(a) Relative PSNR vs. QP



(b) Relative PSNR vs. Bitrate

Figure 5: Video coding performance assessment relative to Original HEVC.

4 VLSI ARCHITECTURES

We aim at the physical realization of pruned designs based on the MRDCT, BAS-2008, and BAS-2013. The MRDCT and BAS-2008 were selected in accordance to the discussion in previous section. The BAS-2013 was also included because it is the base for the only pruned approximate DCT competitor in literature [47]. Such designs were realized in a separable 2-D block transform using two 1-D transform blocks with a transpose buffer between them. Such blocks were designed and simulated, using bit-true cycle-accurate modeling, in Matlab/Simulink. Thereafter, the proposed architecture was ported to Xilinx Virtex-6 field programmable gate array (FPGA) as well as to custom CMOS standard-cell integrated circuit (IC) design. The transform was applied in a row-parallel fashion to the blocks of data and all blocks were 8×8 , irrespective of pruning. When K decreases, the number of null elements in the blocks increases. The row-transformed data were subject to transposition and then the same pruned algorithm was applied, albeit for column direction. Figure 7 shows the architectures for the MRDCT. Remaining designs have similar realizations.

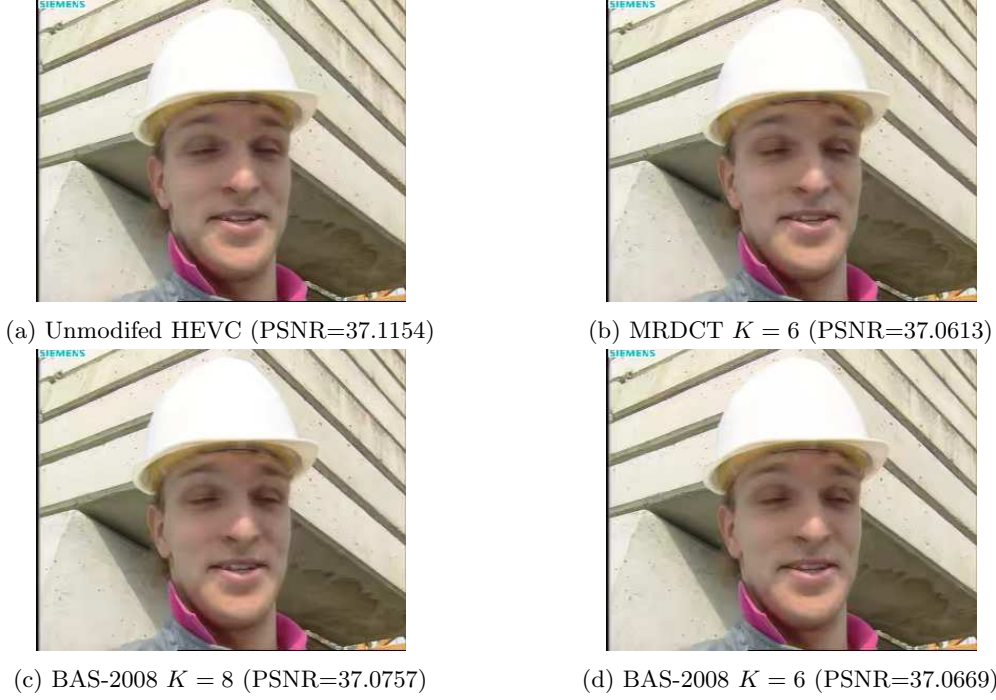


Figure 6: Reconstruct first frame of the “Foreman” video sequence encoded according to considered methods.

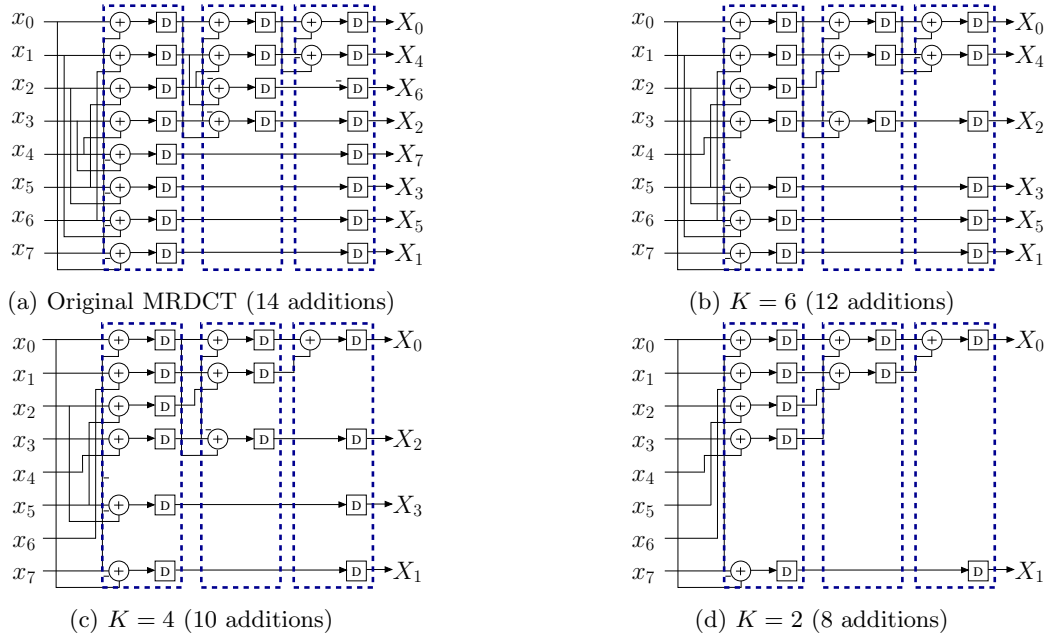


Figure 7: Digital architectures of the MRDCT matrix and pruned MRDCT matrices for $K = 6, 4, 2$.

Table 3: Resource consumption on Xilinx XC6VLX240T-1FFG1156 device

K	CLB	FF	T_{cpd}	F_{max}	D_p
1	107	376	2.263	441.89	0.67
	107	376	2.263	441.89	0.67
	107	376	2.263	441.89	0.67
2	136	568	2.300	434.78	0.97
	203	672	2.600	384.61	1.33
	204	751	2.450	408.10	1.45
3	210	783	2.509	398.56	0.87
	252	956	2.878	347.46	1.74
	263	978	2.534	394.63	2.11
4	247	961	2.946	339.44	1.35
	343	1170	3.100	322.58	2.06
	339	1216	2.900	344.82	2.50
5	290	1123	2.877	347.58	1.70
	362	1331	3.067	326.05	2.76
	377	1374	2.902	344.58	3.13
6	350	1286	2.735	365.63	2.07
	438	1531	3.214	311.13	3.07
	382	1557	2.784	359.19	3.80
7	424	1487	3.300	303.03	2.21
	501	1709	3.286	304.32	3.58
	445	1720	3.432	291.37	3.87
8	445	1696	3.390	294.98	2.74
	559	1962	3.300	303.03	3.85
	517	1910	3.200	312.5	5.07

4.1 FPGA RAPID PROTOTYPES

The pruned architectures were physically realized on a Xilinx Virtex-6 XC6VLX 240T-1FFG1156 FPGA device with fine-grain pipelining for increased throughput. The FPGA realizations were verified using hardware-in-the-loop testing, which was achieved through a JTAG interface. Proposed approximations were verified using more than 10000 test vectors with complete agreement with theoretical values. Evaluation of hardware complexity and real-time performance considered the following metrics: the number of employed configurable logic blocks (CLB), flip-flop (FF) count, critical path delay (T_{cpd}), and the maximum operating frequency (F_{max}) in MHz. The `xflow.results` report file, from the Xilinx FPGA tool flow, led to the reported results. Frequency normalized dynamic power (D_p , in mW/MHz) was estimated using the Xilinx XPower Analyzer software tool. Above measurements are shown in Table 3 for the proposed pruned MRDCT (highlighted in green), the pruned version of the BAS-2008 introduced in [27] (highlighted in blue) and the pruned BAS-2013 introduced in [30].

4.2 ASIC SYNTHESIS

For the ASIC synthesis, the hardware description language code from the Xilinx System Generator FPGA design flow was ported to 45 nm CMOS technology and subject to synthesis using Cadence Encounter. Standard ASIC cells from the FreePDK, which a free open-source cell library at the 45 nm node, was used

Table 4: Resource consumption for CMOS 45 nm ASIC synthesis

K	Area	AT	AT^2	T_{cpd}	F_{max}	D_p
1	0.011	0.011	0.010	0.961	1.040	0.018
	0.011	0.011	0.010	0.961	1.040	0.018
	0.011	0.011	0.010	0.961	1.040	0.018
2	0.017	0.016	0.015	0.962	1.039	0.028
	0.021	0.020	0.020	0.980	1.020	0.035
	0.022	0.022	0.022	0.995	1.005	0.036
3	0.022	0.021	0.020	0.963	1.038	0.038
	0.031	0.030	0.030	0.990	1.010	0.051
	0.029	0.028	0.027	0.981	1.019	0.047
4	0.027	0.027	0.026	0.970	1.030	0.047
	0.037	0.037	0.038	1.016	0.984	0.063
	0.037	0.036	0.036	0.997	1.003	0.059
5	0.032	0.034	0.037	1.075	0.930	0.057
	0.042	0.042	0.043	1.011	0.989	0.069
	0.041	0.041	0.041	1.007	0.993	0.068
6	0.038	0.038	0.037	0.995	1.005	0.067
	0.048	0.048	0.048	1.000	1.000	0.081
	0.046	0.046	0.046	1.008	0.992	0.077
7	0.043	0.047	0.051	1.085	0.921	0.079
	0.053	0.053	0.054	1.014	0.986	0.091
	0.051	0.054	0.057	1.050	0.952	0.087
8	0.046	0.051	0.057	1.103	0.906	0.084
	0.060	0.062	0.065	1.047	0.955	0.104
	0.057	0.057	0.058	1.008	0.992	0.097

for this purpose. The supply voltage of the CMOS realization was fixed at $V_{DD} = 1.1$ V during estimation of power consumption and logic delay. The adopted figures of merit for the ASIC synthesis were: area (A) in mm^2 , area-time complexity (AT) in $\text{mm}^2 \cdot \text{ns}$, area-time-squared complexity (AT^2) in $\text{mm}^2 \cdot \text{ns}^2$, frequency normalized dynamic power (D_p , in mW/MHz), critical path delay (T_{cpd}) in ns, and maximum operating frequency (F_{max}) in GHz. ASIC synthesis results for the proposed pruned MRDCT (highlighted in green), pruned version of the BAS-2008 (highlighted in blue) and the pruned BAS-2013 algorithm are displayed in Table 4.

4.3 DISCUSSION

The FPGA realization of the proposed pruned MRDCT showed a drastic reductions in both area (measured from the number of CLBs) and frequency normalized dynamic power consumption, compared to the full MRDCT. Table 5 shows the percentage reduction of area and frequency-normalized dynamic power for both FPGA implementation and CMOS synthesis for different pruning values. All metrics indicate lower hardware resource consumption when the number of outputs are reduced from 8 to 1. In particular, for $K = 6$, which minimizes the discussed cost function (cf. (11)), we notice a power consumption reduction for approximately 20–25%.

In order to compare the hardware resource consumption of the introduced pruned DCT approximation

Table 5: Percentage reduction in area and dynamic power for FPGA

K	FPGA		ASIC	
	Area %	D_p %	Area %	D_p %
1	71.65	83.11	75.32	76.66
2	54.59	72.29	64.93	66.00
3	44.88	62.33	53.24	54.66
4	30.18	51.94	41.55	43.33
5	19.16	34.63	32.46	34.00
6	3.14	20.77	23.37	24.66
7	1.57	12.12	10.38	12.66

with competing transforms, we physically realized the pruned BAS-2013 algorithm [30] and the pruned BAS-2008 algorithm [27] on the same Xilinx Virtex-6 XC6VLX240T-1FFG1156 device and submitted it to synthesis using ASIC 45 nm CMOS technology. By comparing the results in Table 3 and 4, it can be seen that the proposed transform discussed here outperforms both pruned BAS-2008 and pruned BAS-2013 in terms of hardware resource consumption, and power consumption while is in par in terms of speed as well.

5 CONCLUSION

In this paper, we present a set of 8-point pruned DCT approximations derived from state-of-the-art methods. All possible frequency-domain pruning schemes were considered and analyzed in terms of arithmetic complexity, energy compaction in the transform-domain, and image compression performance. A new combined metric was defined considering the 2-D arithmetic complexity and average values of PSNR and SSIM. The pruned transform based on MRDCT presented the lowest arithmetic complexity and the showed competitive performance. Thus, the pruned MRDCT approximations were digitally implemented using both Xilinx FPGA tools and CMOS 45 nm ASIC technology. The proposed pruned transforms demonstrated practical relevance in image/video compression. The proposed algorithms are fully compatible with modern codecs. We have embedded the proposed methods into a standard HEVC reference software [59]. Results presented very low qualitative and quantitative degradation at a considerable lower computational cost.

Additionally, low-complexity designs are required in several contexts where very high quality imagery is not a strong requirement, such as: environmental monitoring, habitat monitoring, surveillance, structural monitoring, equipment diagnostics, disaster management, and emergency response [61]. All above contexts can benefit of the proposed tools when embedded into wireless sensors with low-complexity codecs and low-power hardware [62].

We summarize the contributions of the present work:

- The pruning approach for DCT approximations was generalized by not only considering all possible pruning variations but also investigating a wide range of DCT approximations;
- An analysis covering all cases under different figures of merit, including arithmetic complexity and image quality measures was presented;
- A combined figure of merit to guide the decision making process in terms hardware realization was introduced;

- The 2-D case was also analyzed and concluded that the pruning approach is even better suited for 2-D transforms.
- The considered pruned DCT approximation was implemented using Xilinx FPGA tools and synthesized using CMOS 45 nm ASIC technology. Such implementations demonstrated the low resource consumption of the proposed pruned transform.

ACKNOWLEDGEMENTS

This work was partially supported by CNPq, FACEPE, and FAPERGS (Brazil), and by the College of Engineering at the University of Akron, Akron, OH, USA.

REFERENCES

- [1] N. Ahmed and K. R. Rao, *Orthogonal Transforms for Digital Signal Processing*. Springer, 1975.
- [2] R. E. Blahut, *Fast Algorithms for Signal Processing*. Cambridge University Press, 2010.
- [3] G. Wallace, “The JPEG still picture compression standard,” *IEEE Transactions on Consumer Electronics*, vol. 38, no. 1, pp. xviii–xxxiv, 1992.
- [4] D. J. L. Gall, “The MPEG video compression algorithm,” *Signal Processing: Image Communication*, vol. 4, pp. 129–140, 1992.
- [5] N. Roma and L. Sousa, “Efficient hybrid DCT-domain algorithm for video spatial downscaling,” *EURASIP Journal on Advances in Signal Processing*, vol. 2007, no. 2, pp. 30–30, 2007.
- [6] International Organisation for Standardisation, “Generic coding of moving pictures and associated audio information – Part 2: Video,” ISO, ISO/IEC JTC1/SC29/WG11 - Coding of Moving Pictures and Audio, 1994.
- [7] International Telecommunication Union, “ITU-T recommendation H.261 version 1: Video codec for audiovisual services at $p \times 64$ kbits,” ITU-T, Tech. Rep., 1990.
- [8] M. L. Liou, “Visual telephony as an ISDN application,” *IEEE Communications Magazine*, vol. 28, pp. 30–38, 1990.
- [9] International Telecommunication Union, “ITU-T recommendation H.263 version 1: Video coding for low bit rate communication,” ITU-T, Tech. Rep., 1995.
- [10] T. Wiegand, G. J. Sullivan, G. Bjontegaard, and A. Luthra, “Overview of the H.264/AVC video coding standard,” *IEEE Transactions on Circuits and Systems for Video Technology*, vol. 13, no. 7, pp. 560–576, Jul. 2003.
- [11] J. V. Team, “Recommendation H.264 and ISO/IEC 14 496–10 AVC: Draft ITU-T recommendation and final draft international standard of joint video specification,” ITU-T, Tech. Rep., 2003.
- [12] International Telecommunication Union, “High efficiency video coding: Recommendation ITU-T H.265,” ITU-T Series H: Audiovisual and Multimedia Systems, Tech. Rep., 2013.
- [13] M. T. Pourazad, C. Dautre, M. Azimi, and P. Nasiopoulos, “HEVC: The new gold standard for video compression: How does HEVC compare with H.264/AVC?” *IEEE Consumer Electronics Magazine*, vol. 1, no. 3, pp. 36–46, Jul. 2012.
- [14] J.-S. Park, W.-J. Nam, S.-M. Han, and S. Lee, “2-D large inverse transform (16×16 , 32×32) for HEVC (High Efficiency Video Coding),” *Journal of Semiconductor Technology and Science*, vol. 2, pp. 203–211, 2012.

- [15] J.-R. Ohm, G. J. Sullivan, H. Schwarz, T. K. Tan, and T. Wiegand, "Comparison of the coding efficiency of video coding standards - including High Efficiency Video Coding (HEVC)," *IEEE Transactions on Circuits and Systems for Video Technology*, vol. 22, no. 12, pp. 1669–1684, Dec. 2012.
- [16] U. S. Potluri, A. Madanayake, R. J. Cintra, F. M. Bayer, S. Kulasekera, and A. Edirisuriya, "Improved 8-point approximate DCT for image and video compression requiring only 14 additions," *IEEE Transactions on Circuits and Systems I*, vol. 61, no. 6, pp. 1727–1740, 2014.
- [17] G. J. Sullivan, J.-R. Ohm, W.-J. Han, and T. Wiegand, "Overview of the high efficiency video coding (HEVC) standard," *IEEE Transactions on Circuits and Systems for Video Technology*, vol. 22, no. 12, pp. 1649–1668, Dec. 2012.
- [18] W. H. Chen, C. Smith, and S. Fralick, "A fast computational algorithm for the discrete cosine transform," *IEEE Transactions on Communications*, vol. 25, no. 9, pp. 1004–1009, Sep. 1977.
- [19] H. S. Hou, "A fast recursive algorithm for computing the discrete cosine transform," *IEEE Transactions on Acoustic, Signal, and Speech Processing*, vol. 6, no. 10, pp. 1455–1461, 1987.
- [20] Y. Arai, T. Agui, and M. Nakajima, "A fast DCT-SQ scheme for images," *Transactions of the IEICE*, vol. E-71, no. 11, pp. 1095–1097, Nov. 1988.
- [21] C. Loeffler, A. Ligtenberg, and G. S. Moschytz, "Practical fast 1-D DCT algorithms with 11 multiplications," *ICASSP International Conference on Acoustics, Speech, and Signal Processing*, vol. 2, pp. 988–991, 1989.
- [22] E. Feig and S. Winograd, "Fast algorithms for the discrete cosine transform," *IEEE Transactions on Signal Processing*, vol. 40, no. 9, pp. 2174–2193, 1992.
- [23] V. Britanak, P. Yip, and K. R. Rao, *Discrete Cosine and Sine Transforms*. Academic Press, 2007.
- [24] S. Winograd, *Arithmetic Complexity of Computations*. CBMS-NSF Regional Conference Series in Applied Mathematics, 1980.
- [25] T. I. Haweel, "A new square wave transform based on the DCT," *Signal Processing*, vol. 82, pp. 2309–2319, 2001.
- [26] K. Lengwehasatit and A. Ortega, "Scalable variable complexity approximate forward DCT," *IEEE Transactions on Circuits and Systems for Video Technology*, vol. 14, no. 11, pp. 1236–1248, Nov. 2004.
- [27] S. Bouguezel, M. O. Ahmad, and M. N. S. Swamy, "Low-complexity 8×8 transform for image compression," *Electronics Letters*, vol. 44, no. 21, pp. 1249–1250, Sep. 2008.
- [28] R. J. Cintra and F. M. Bayer, "A DCT approximation for image compression," *IEEE Signal Processing Letters*, vol. 18, no. 10, pp. 579–582, Oct. 2011.
- [29] S. Bouguezel, M. O. Ahmad, and M. N. S. Swamy, "A fast 8×8 transform for image compression," in *2009 International Conference on Microelectronics (ICM)*, Dec. 2009, pp. 74–77.
- [30] —, "Binary discrete cosine and Hartley transforms," *IEEE Transactions on Circuits and Systems I: Regular Papers*, vol. 60, no. 4, pp. 989–1002, 2013.
- [31] R. J. Cintra, F. M. Bayer, and C. J. Tablada, "Low-complexity 8-point DCT approximations based on integer functions," *Signal Processing*, vol. 99, pp. 201–214, 2014.
- [32] L. Makkaoui, V. Lecuire, and J. Moureaux, "Fast zonal DCT-based image compression for wireless camera sensor networks," *2nd International Conference on Image Processing Theory Tools and Applications (IPTA)*, pp. 126–129, 2010.
- [33] A. Docef, "The quantized DCT and its application to DCT-based video coding," *IEEE Transactions on Image Processing*, vol. 11, pp. 177–187, 2002.

- [34] K. R. Rao and P. Yip, *Discrete Cosine Transform: Algorithms, Advantages, Applications*. San Diego, CA: Academic Press, 1990.
- [35] N. Ahmed, T. Natarajan, and K. R. Rao, "Discrete cosine transform," *IEEE Transactions on Computers*, vol. C-23, no. 1, pp. 90–93, Jan. 1974.
- [36] K. R. Rao and P. Yip, *The Transform and Data Compression Handbook*. CRC Press LLC, 2001.
- [37] H. Malepati, *Digital Media Processing: DSP Algorithms Using C (Google e-Libro)*. Newnes, 2010.
- [38] Y.-M. Huang, J.-L. Wu, and C.-L. Chang, "A generalized output pruning algorithm for matrix-vector multiplication and its application to compute pruning discrete cosine transform," *IEEE Transactions on Signal Processing*, vol. 48, pp. 561–563, 2000.
- [39] L. Wang, X. Zhou, G. Sobelman, and R. Liu, "Generic mixed-radix FFT pruning," *IEEE Signal Processing Letters*, vol. 19, no. 3, pp. 167–170, March 2012.
- [40] R. Airoldi, O. Anjum, F. Garzia, A. M. Wyglinski, and J. Nurmi, "Energy-efficient fast Fourier transforms for cognitive radio systems," *IEEE Micro*, vol. 30, no. 6, pp. 66–76, Nov 2010.
- [41] P. Whatmough, M. Perrett, S. Isam, and I. Darwazeh, "VLSI architecture for a reconfigurable spectrally efficient FDM baseband transmitter," *IEEE Transactions on Circuits and Systems I: Regular Papers*, vol. 59, no. 5, pp. 1107–1118, May 2012.
- [42] J.-H. Kim, J.-G. Kim, Y.-H. Ji, Y.-C. Jung, and C.-Y. Won, "An islanding detection method for a grid-connected system based on the Goertzel algorithm," *IEEE Transactions on Power Electronics*, vol. 26, no. 4, pp. 1049–1055, Apr. 2011.
- [43] I. Carugati, S. Maestri, P. Donato, D. Carrica, and M. Benedetti, "Variable sampling period filter PLL for distorted three-phase systems," *Power Electronics, IEEE Transactions on*, vol. 27, no. 1, pp. 321–330, Jan. 2012.
- [44] Z. Wang, "Pruning the fast discrete cosine transform," *IEEE Transactions on Communications*, vol. 39, no. 5, pp. 640–643, May 1991.
- [45] A. Skodras, "Fast discrete cosine transform pruning," *IEEE Transactions on Signal Processing*, vol. 42, no. 7, pp. 1833–1837, Jul 1994.
- [46] V. Lecuire, L. Makkaoui, and J.-M. Moureaux, "Fast zonal DCT for energy conservation in wireless image sensor networks," *Electronics Letters*, vol. 48, no. 2, pp. 125–127, 2012.
- [47] N. Kouadria, N. Doghmane, D. Messadeg, and S. Harize, "Low complexity DCT for image compression in wireless visual sensor networks," *Electronics Letters*, vol. 49, no. 24, pp. 1531–1532, 2013.
- [48] P. Meher, S. Y. Park, B. Mohanty, K. S. Lim, and C. Yeo, "Efficient integer DCT architectures for HEVC," *Circuits and Systems for Video Technology, IEEE Transactions on*, vol. 24, no. 1, pp. 168–178, Jan. 2014.
- [49] A. Oppenheim and R. Schaffer, *Discrete-Time Signal Processing*, 3rd ed. Pearson, 2010.
- [50] F. M. Bayer and R. J. Cintra, "DCT-like transform for image compression requires 14 additions only," *Electronics Letters*, vol. 48, no. 15, pp. 919–921, 19 2012.
- [51] D. F. Elliot and K. R. Rao, *Fast Transforms: Algorithms, Analyses, Applications*. Academic Press, 1982.
- [52] K. M. Abadir and J. R. Magnus, *Matrix Algebra*. Cambridge University Press, 2005.
- [53] V. Bhaskaran and K. Konstantinides, *Image and Video Compression Standards*. Boston: Kluwer Academic Publishers, 1997.

- [54] USC-SIPI Image Database. Signal and Image Processing Institute. University of Southern California. [Online]. Available: <http://sipi.usc.edu/database/>
- [55] W. B. Pennebaker and J. L. Mitchell, *JPEG Still Image Data Compression Standard*. New York, NY: Van Nostrand Reinhold, 1992.
- [56] Z. Wang, A. C. Bovik, H. R. Sheikh, and E. P. Simoncelli, "Image quality assessment: from error visibility to structural similarity," *IEEE Transactions on Image Processing*, vol. 13, no. 4, pp. 600–612, Apr. 2004.
- [57] L. Zhang and H. Li, "SR-SIM: A fast and high performance iqa index based on spectral residual," *19th IEEE International Conference on Image Processing (ICIP)*, pp. 1473 – 1476, 2012.
- [58] M. Ehrgott, *Multicriteria Optimization*, ser. Lecture Notes in Economics and Mathematical Systems. Springer-Verlag GmbH, 2005.
- [59] JCT-VC. (2015) HM 10.0. <https://hevc.hhi.fraunhofer.de/>. Joint Collaborative Team on Video Coding (JCT-VC). Fraunhofer Heinrich Hertz Institute. [Online]. Available: <https://hevc.hhi.fraunhofer.de/>
- [60] xiph.org. (2015) <https://media.xiph.org/video/derf/>. Xiph.org video test media. [Online]. Available: <https://media.xiph.org/video/derf/>
- [61] N. Kimura and S. Latifi, "A survey on data compression in wireless sensor networks," *International Conference on Information Technology: Coding and Computing, ITCC*, vol. 2, pp. 8–13, 2005.
- [62] I. F. Akyildiz, T. Melodia, and K. R. Chowdhury, "A survey on wireless multimedia sensor networks," *Computer Networks*, vol. 51, pp. 921–960, 2007.